https://doi.org/10.1002/adfm.201902784

Advanced Functional Materials - ***2019***
DOI: 10.1002/adfm.201902784

Introducing a Non-Volatile N-Type Dopant Drastically Improves Electron Transport in Polymer and Small-Molecule Organic Transistors

Julianna Panidi, Jaspreet Kainth, Alexandra F. Paterson, Simeng Wang, Leonidas Tsetseris, Abdul-Hamid Emwas, Martyn A. McLachlan, Martin Heeney, Thomas D. Anthopoulos**

J. Panidi, Prof. T. D. Anthopoulos
Department of Physics and Centre for Plastic Electronics
Imperial College London
South Kensington, London SW7 2AZ (UK)

Jaspreet Kainth, Dr. M. A. McLachlan
Department of Materials and Centre for Plastic Electronics
Imperial College London
South Kensington, London SW7 2AZ (UK)

Prof. L. Tsetseris
Department of Physics
National Technical University of Athens
Athens GR-15780, Greece

Dr. Simeng Wang, Prof. M. Heeney
Department of Chemistry and Centre for Plastic Electronics
Imperial College London
South Kensington, London SW7 2AZ (UK)
E-mail: m.heeney@imperial.ac.uk

Dr. A.-H. Emwas
Core Labs, King Abdullah University of Science and Technology
Thuwal 23955-6900, Saudi Arabia

Dr. A. F. Paterson, Prof. T. D. Anthopoulos
King Abdullah University of Science and Technology (KAUST)
Division of Physical Sciences and Engineering,
Thuwal 23955-6900, Saudi Arabia
E-mail: thomas.anthopoulos@kaust.edu.sa

Keywords: organic semiconductors; organic transistor; electron transport; molecular doping; n-type dopant

https://doi.org/10.1002/adfm.201902784

Abstract

Molecular doping is a powerful yet challenging technique for enhancing charge transport in organic semiconductors. Whilst there is a wealth of research on p-type dopants, work on their n-type counterparts is comparatively limited. Here, we report on the previously unexplored n-dopant (12a,18a)-5,6,12,12a,13,18,18a,19-octahydro-5,6-dimethyl-13,18[1',2']-benzenobisbenzimidazo [1,2-b:2',1'-d]benzo[i][2.5]benzodiazocine potassium triflate adduct (DMBI-BDZC), and its application in organic thin-film transistors (OTFTs). Two different high electron mobility organic semiconductors, namely the polymer poly[[N,N′-bis(2-octyldodecyl)-naphthalene-1,4,5,8-bis(dicarboximide)-2,6-diyl]-alt-5,5′-(2,2′-bithiophene)] (N2200) and the small molecule naphthalene diimides fused with 2- (1,3-dithiol-2-ylidene)malononitrile groups (NDI-DTYM2) (NDI3HU-DTYM2), are used to study the effectiveness of DMBI-BDZC as n-dopant and its impact on the device operation. N-doping of both semiconductors results in OTFTs with to improved electron mobility (up to 1.1 cm^2/Vs), reduced threshold voltage and lower contact resistance. The impact of DMBI-BDZC incorporation is particularly evident in the temperature-dependence of the electron transport in both semiconductors, where a significant reduction in the activation energy due trap deactivation is observed. Electron paramagnetic resonance measurements supports the n-doping activity of DMBI-BDZC in both semiconductors upon blending. This finding is corroborated by density functional theory calculations, which highlights ground-state electron transfer as the main doping mechanism. The work highlights DMBI-BDZC as a promising n-type molecular dopant for organic semiconductors and its application in OTFTs, solar cells, photodetectors and thermoelectrics.

1. Introduction

Over the past few decades organic semiconductors (OSCs) have become the material of choice for a wide range of emerging optoelectronic applications a few examples of which include organic light emitting diodes (OLEDs)[1–3], organic photovoltaics (OPVs)[4,5] and organic thin-film transistors (OTFTs) [6–8]. During this time, increasing effort has been directed towards tuning OSCs' properties including their processing characteristics and charge carrier transport primarily via the development of new materials and their application in devices with improved operating characteristics.[8,9] In parallel, alternative approaches towards improving the device performance have also been exploited, one of which is the tuning of the charge transport via intentional chemical doping.[10] For instance, in

the case of OLEDs and OPVs, doping of the electron transporting (ETL) and hole transporting layers (HTL) was proven an extremely valuable technology as it enabled the development of devices with improved efficiencies.[11–18]

In the case of OTFTs, intentional doping is also known to result in improved device parameters, including reduced contact resistance, improved bias-stability and higher charge carrier mobility.[10,19] However, the characteristically low doping efficiencies and microstructural disruption of the host semiconductor upon introduction of the often bulky molecular dopants are two effects that have so far inhibited widespread adoption of the technology in OTFTs.[20,21] A further limitation is the fact that although numerous studies have been performed on p-type doping of organic semiconductors,[20,22–31] research on n-type dopants is rather limited.[32–35] This is because doping via the traditional ground-state integer charge transfer (ICT) process requires the donation of an electron from the highest occupied molecular orbital (HOMO) of the dopant, to the lowest unoccupied lower orbital (LUMO) of the host semiconductor. This rather stringent condition makes the synthesis, and/or identification, of n-type molecular dopants with a high enough HOMO –that are also air-stable and easy to handle– challenging.[36–42]

To tackle this bottleneck, alternative n-doping mechanisms have been proposed. [33,43] One such example is the small molecule benzimidazole−dimethylbenzenamine (N-DMBI), which has been shown to n-dope a variety of semiconductors by transferring a hydride atom to the acceptor molecule.[44–47] Another successful example of non-traditional n-doping is via the addition of salts such as tetrabutylammonium fluoride (TBAF) and tetrabutylammonium hydroxide (TBAOH) the introduction of which results in the formation of radical anions which in turn dope the host semiconductor.[34,48] The latter approach has proven efficient in n-doping of the polymer semiconductor poly[[N,N′-bis(2-octyldodecyl)-naphthalene-1,4,5,8-bis(dicarboximide)-2,6-diyl]-alt-5,5′-(2,2′-bithiophene)] (P(NDI2OD-T2)), hereafter abbreviated N2200, and was shown capable of producing OTFTs with a maximum electron mobility value of 0.67 $cm^2 V^{-1} s^{-1}$.[48] Given the notable

lack of n-type molecular dopants, efforts towards identification and/or synthesis of new n-dopants has been intensifying.

Herein we report on the use of a previously unidentified n-type dopant namely (12a,18a)-5,6,12,12a,13,18,18a,19-octahydro-5,6-dimethyl-13,18[1',2']-benzenobisbenzimidazo[1,2-b:2',1'-d]benzo[i][2.5]benzodiazocine potassium triflate adduct (DMBI-BDZC)[49] for the development of high performance solution-processed OTFTs. DMBI-BDZC has been used to generate chiral rhodium (I) bis(N-heterocyclic carbene) complexes by C=C bond cleavage.[49] Such complexes are useful enantioselective catalysts.[50] However, our interest in DMBI-BDZC lies in its electron rich enetetramine core, since such electron rich alkenes are known to serve as n-type dopants.[42] Tetrakis(dimethylamino)ethylene is a classical dopant of this class,[51] but it is a volatile liquid which reacts with atmospheric oxygen.[52] The high volatility can also lead to stability issues and de-doping on storage[53] and thus such drawbacks have limited its application as a molecular dopant. DMBI-BDZC, on the other hand, is a low vapour pressure crystalline solid, which may overcome these issues. To investigate its potential as a dopant, two different organic semiconductors namely the polymer poly[[N,N′-bis(2-octyldodecyl)-naphthalene-1,4,5,8-bis(dicarboximide)-2,6-diyl]-alt-5,5′-(2,2′-bithiophene)] (N2200) and the small molecule naphthalene diimides fused with 2- (1,3-dithiol-2-ylidene)malononitrile groups (NDI-DTYM2) (NDI3HU-DTYM2),[54] are used as the prototypical semiconductors to study the effectiveness of DMBI-BDZC as n-type dopant. Electron paramagnetic resonance (EPR) measurements reveal the formation of radical species in both semiconductors upon DMBI-BDZC addition. Further evidence of n-type doping are provided by OTFT measurements performed as a function of temperature, which shows a characteristic reduction of the activation energy upon n-doping and an increase in the electron mobility. Finally, microstructural analysis of the OSC channel via atomic force microscopy (AFM) and X-ray diffraction (XRD) measurements indicates that DMBI-BDZC does not disrupt the packing motif of the N2200 polymer, whereas minor influence is observed for the NDI3HU-DTYM2.

2. Results and Discussion

The molecular structure together with the calculated frontier orbitals energies for DMBI-BDZC are shown in **Figure 1a**. Here, the LUMO and HOMO levels were calculated via Density Functional Theory (DFT) yielding -0.74 eV and -3.84 eV, respectively. **Figure 1b** and **1c** presents the chemical structure of the organic semiconductors N2200 and NDI3HU-DTYM2, both renowned for their high field-effect electron mobility (μ)[34,55–57], along with their energy levels as predicted by DFT calculations. The HOMO/LUMO levels for N2200 and NDI3HU-DTYM2 were found -5.80/-3.80 eV and -7.09/-4.80 eV, respectively (**Figure S1**) consistent with previous reports (which gave a range of -4.00 eV to -3.80 eV for the LUMO level of N2200).[58–64] As can be seen, the HOMO of DMBI-BDZC (-3.84 eV) is significantly higher than the LUMO of NDI3HU-DTYM2 (-4.80 eV) and comparable to that of N2200 (-3.80 eV). It should also be mentioned that the N2200 LUMO energy can be slightly different (it broadens to a band with a lower energy minimum) for an extended polymer chain in a crystal. Overall, these energetics suggest that ground-state integer charge transfer (ICT) between the dopant and the two semiconductors is indeed a plausible mechanism that could lead to n-type doping.

2.1 Electron paramagnetic resonance (EPR) measurements

EPR measurements were carried out in order to assess whether DMBI-BDZC functions as an n-type dopant for N2200 and NDI3HU-DTYM2. The EPR method can directly detect the presence of unpaired or free electrons and it has been used extensively in the field of organic semiconductors to evaluate doping.[23,34] In brief, a magnetic field was used to promote the transition of unpaired electrons present in optimized (in terms of OTFTs performance) n-doped layers, as compared to the pristine (0 mol%) semiconductor systems. **Figure 2a** and **2c** show the measured EPR signal for N2200 and NDI3HU-DTYM2, respectively. As evident from these plots, the pristine samples show no EPR signal indicative of their intrinsic nature. However, when a small amount, 0.2 mol% for the N2200 and 0.5 mol% for the NDI3HU-DTYM2, of DMBI-BDZC is introduced to the system, a clear

signal attributable to paramagnetic radical species is observed in both semiconductors. The latter observation is consistent with what would be expected upon successful n-doping.[65–67]. **Figures 2b** and **2d**, depicts the charge transfer process between the dopant and the host semiconductor. Despite the relatively small energy offset (ΔE) between the dopant's HOMO and the LUMO of N2200 – the main driving force for the electron transfer process – the dopant can clearly induce free electrons in N2200 (**Figure 2a**). In the case of NDI3HU-DTYM2 (**Figure 2d**), ΔE is large (≈1 eV) leading to clear n-type doping as evident in the EPR data of **Figure 2c**. On the basis of the EPR measurements, we conclude that DMBI-BDZC can indeed successfully n-dope both organic semiconductors.

2.1 Field-effect transistor measurements

Recent studies have shown that the operating characteristics of OTFTs can be improved via molecular doping,[20,27,34] with the transistor device itself providing an excellent tool for studying molecular doping in OSCs.[10,68–70] To study the impact of DMBI-BDZC on the charge transport characteristics of N2200 and NDI3HU-DTYM2, we fabricated bottom-contact, top-gate (BC-TG) OTFTs (see inset in **Figure 3a**). **Figure 3a-b** show representative transfer characteristics (I_D *vs.* V_G) of the resultant N2200:DMBI-BDZC (0-1 mol%) and NDI3HU-DTYM2:DMBI-BDZC (0-2 mol%) OTFTs, respectively, together with the corresponding $I_D^{0.5}$ *vs.* V_G plots, from which the threshold voltage (V_T) and electron mobility (μ) can both be determined. Evidently, DMBI-BDZC has a notable impact on the OTFTs based on both semiconductors with clear signs of n-type doping. Specifically, V_T shifts towards more negative values, an effect associated with trap filling at the dielectric/semiconductor interface.[71]

Doping with DMBI-BDZC is also found to have a profound effect on the electron transport characteristics of both OTFTs. **Figure 3c** and **3d** show the evolution of the electron mobility, calculated in both linear (μ_{lin}) and saturation (μ_{sat}) regime, and V_T as a function of DMBI-BDZC concentration. For N2200:DMBI-BDZC-based OTFTs, both μ_{lin} and μ_{sat} are found to increase from 0.1 and 0.2 $cm^2\ V^{-1}\ s^{-1}$ to their maximum magnitude of 0.4 and 0.7 $cm^2\ V^{-1}\ s^{-1}$, respectively, for 0.2

mol% dopant concentration. A similar behaviour is seen in NDI3HU-DTYM2:DMBI-BDZC transistors, where both μ_{lin} and μ_{sat} increase from 0.4 and 0.8 $cm^2\ V^{-1}\ s^{-1}$, respectively, to their maximum values of 0.8 and 1.1 $cm^2\ V^{-1}\ s^{-1}$ for an optimum dopant concentration of 0.5 mol%. As the dopant concentration increases beyond the optimal value, the electron mobility reduces for both semiconductors. Moreover, a drastic reduction in the threshold voltage (V_T) for the N2200:DMBI-BDZC devices (**Figure 3c**) is observed upon doping with 0.1 mol% beyond which it remains unchanged. A similar dependence of V_T on dopant concentration is observed for the NDI3HU-DTYM2:DMBI-BDZC transistors (**Figure 3d**). From the transfer curves one can also notice the characteristic decrease in the current on-off ratio ($I_{ON/OFF}$) in both N2200:DMBI-BDZC and NDI3HU-DTYM2:DMBI-BDZC OTFTs (**Figure 3c**). The $I_{ON/OFF}$ degradation is primarily attributed to the gradual increase in the channel off current (I_{OFF}) with increasing dopant concentration. **Figures S2** and **S3** show the transfer and output characteristics for best performing pristine and doped OTFTs based on N2200:DMBI-BDZC and NDI3HU-DTYM2:DMBI-BDZC OTFTs, respectively.

Next, we investigated the influence of DMBI-BDZC on contact resistance (R_C) – an additional important device parameter known to benefit from molecular doping.[20] R_C is known to inhibit overall device performance and accurate parameter extraction. Several groups are working to identify ways to reduce the R_C for organic thin film transistors reaching values of 200 Ωcm[72] or even below by contact engineering[73]. Doping the organic semiconducting layer is another way to solve the problem of parasitic R_C in OTFTs. **Figure 3e** shows the evolution of R_C with increasing V_G for the pristine and best performing n-doped semiconductors calculated using the transmission line method (TLM).[74] In N2200 OTFTs, R_C is found to improve from 1.8×10^6 to 4.8×10^5 Ω at V_G =10 V. In the case of NDI3HU-DTYM2 devices, n-doping with DMBI-BDZC is seen to change the R_C dependency on V_G, decreasing R_C by approximately one order of magnitude at low V_G (V_G = 10 V), but approaching same values at higher V_G. Overall, the charge transport data show that DMBI-BDZC act as n-dopant which in turn helps to improve the OTFT performance.

To gain further insight into the impact of n-type doping on electron transport, the transfer characteristics were recorded over the temperature range of 77 to 310 K for both pristine and optimally doped N2200 and NDI3HU-DTYM2 systems (**Figure S4**). These measurements enabled the estimation of the activation energy (E_A) for electron transport at different bias conditions and dopant concentrations. Here, we particularly focus on studying the impact of DMBI-BDZC addition on E_A. We hypothesize that the observed n-doping effect in both semiconductors will deactivate certain trap states, hence helping to reduce E_A. Analysis of E_A was performed within the framework of the Multiple Trapping and Release (MTR) model, which relates the effective mobility (μ_{eff}) –i.e. the average μ of both mobile and trapped charges measured in a device– with temperature (T), as shown in **Eq. 1**:[75]

$$\mu_{eff} \approx \mu_0 exp\left(\frac{-E_A}{k_B T}\right) \quad (1)$$

where, k_B is the Boltzmann constant and μ_0 is a mobility prefactor. The activation energy of μ_{eff} can be considered as the trap energy level (E_T) relative to the transport level (E_V) given as E_A=E_T-E_V. In real systems, however, trap states are often distributed across a range of energies rather than in a single level, hence making charge transport analysis more elaborate.

Figure 4a-d show the Arrhenius plots of μ_{eff} *vs.* 1000/T for the pristine and optimally doped N2200 and NDI3HU-DTYM2-based OTFTs, recorded at different V_G. Both systems show temperature activated electron transport with two clearly distinguishable conduction regimes; one at high and one at low temperatures. This behaviour is commonly attributed to the temperature dependent charge hopping transport in organic semiconductors.[48,76–78] In N2200-based OTFTs, the temperature that demarcates the high from the low temperature transport regimes is ≈193 K for the pristine polymer and ≈178 K for the best performing doped polymer (with 0.2 mol% DMBI-BDZC) OTFT - both highlighted by the shaded areas in **Figure 4a-b**. For both pristine and n-doped N2200 devices, the two transport regimes appear to be well defined with the transition temperature remaining largely unchanged with increasing V_G. We note, however, that the electron mobility in pristine N2200

transistors varies over three orders of magnitude from a maximum value of 0.1 $cm^2 V^{-1} s^{-1}$ (300 K) to a minimum of $\approx 10^{-4}$ $cm^2 V^{-1} s^{-1}$ (78 K) (**Figure 4a**).

N-doping of N2200 with DMBI-BDZC (0.2 mol%) affects the electron transport significantly with the μ_{eff} exhibiting a smaller dependence on temperature and its value varying between ≈0.5 and $\approx 10^{-2}$ $cm^2 V^{-1} s^{-1}$, at 300 and 78 K, respectively (**Figure 4b**). We employed **Eq. 1** to quantify this difference by calculating the E_A in the higher temperature regime for both pristine and n-doped N2200 OTFTs at different V_G (**Figure 4e**). Evidently, n-doping reduces E_A by almost 50 meV from its initial and maximum value of 170 meV (pristine N2200), down to 124 meV (0.2 mol%) calculated at V_G = 30 V. We ascribe this reduction in E_A to trap filling upon doping and the associated shift in the Fermi energy level towards the LUMO, in agreement with previous reports.[79] At $V_G \geq 75$ V, the E_A for the pristine and n-doped N2200 OTFTs converge to a minimum value of ≈88 meV. This observation suggests that introduction of excess electrons via gate-field or molecular doping has a similar effect despite the lower μ_{eff} measured for the pristine N2200 transistors. We do stress, however, that additional synergistic effects of doping, such as reduced contact resistance and lowering of the V_T, may also be at play and cannot be excluded.[20,70]]

The impact of n-doping of NDI3HU-DTYM2 transistors with DMBI-BDZC (0.5 mol%) (**Figure 4c-d**), on the other hand, appears to be less dramatic with the E_A for the pristine NDI3HU-DTYM2 transistor reducing from 26 to 15 meV, with increasing V_G. The corresponding E_A values for the n-doped NDI3HU-DTYM2 transistors are significantly lower and reduce from 24 meV for the pristine channel to approximately 13 meV for the n-doped devices (**Figure 4f**). A sin the case of N2200, we attribute the reduction in E_A to the deactivation of electron trap states. The noticeable small effect of n-doping on NDI3HU-DTYM2-based transistors is most likely attribute the highly crystalline nature of layers and the tendency to expel the dopant molecules away from the lattice upon nucleation and growth during layer solidification. Nevertheless, the impact of n-doping is significant and clearly measurable further corroborating the role of DMBI-BDZC as a promising n-type molecular dopant.

The reduction in both threshold voltage and activation energy in the doped systems, suggests that DMBI-BDZC is filling trap states in the semiconducting layer, by the free holes generated. Thus the trap density (N_{tr})[80] and the trap concentration (D_{tr}) in the organic films were extracted from the transfer curves (**Figure 3**). **Figure S5** shows the relative variation of the ΔN_{tr} and ΔD_{tr} with increasing DMBI-DBZC concentration for both semiconductors. For the N2200, both N_{tr} and D_{tr} decrease by introducing the dopant molecules. This result is consistent with the reduction in the activation energy of ≈50 meV upon doping (**Figure 4c**) and the reduced threshold voltage and contact resistance **(Figure 3c-d)**. Furthermore, analysis of the NDI3HU-DTYM2:DMBI-BDZC devices shows that the trap concentration is not affected as much as in the N2200 devices; this evidence was also showed in the activation energy analysis (**Figure 4f**). The trap density, on the hand, decreases when 0.1-0.5 mol% of DMBI-BDZC were added, followed by a sharp increase at higher doping concentrations. This observation is likely related to structural defects induced in the semiconductor layer upon doping in agreement with previous reports. [34][81]

2.3 Impact of doping on organic semiconductor layer morphology

Although EPR and low temperature measurements suggest integer charge transfer as the main process responsible for the n-doping observed, charge transport in organic semiconductors is known to dependent on the layer microstructure. Therefore, it is important to investigate the impact of the dopant on the semiconductor layer morphology. **Figure 5a** shows atomic force microscopy (AFM) topography images for the pristine (0 mol%) and n-doped (0.1-1 mol%) N2200 layers. All films show a similar fibril-type surface microstructure. However, a significant shift by ≈2 nm in the height histogram towards lower height values upon doping (**Figure 5b**) is observed indicating that addition of DMBI-BDZC in N2200 leads to the formation of smoother layers. This is further supported by the evolution of the root mean square (RMS) surface roughness values (**Figure 5c**), which decrease upon doping (0.2 mol%) and remains constant for higher dopant concentrations.

X-ray diffraction (XRD) measurements were also used to further examine the impact of DMBI-BDZC on OSCs crystallinity. **Figure 5d** shows the diffraction patterns obtained in the range 2-25^{o} degrees in 2θ for the pristine N2200 and doped N2200:DMBI-BDZC (dopant concentration in the range 0-2 mol%) layers. N2200 exhibits lamellar structures with the characteristic diffraction peaks (100) and (200) at 2θ = 3.67° and 7.22°, respectively, and a π- π stacking peak (010) at 2θ = 22.92°, corresponding to a lamellar packing distances of 2.41 and 1.22 nm and a π- π stacking distance of ≈0.39 nm, in agreement with published data.[34] No significant differences are observed between pristine and doped films suggesting that the packing of the N2200 polymer is not affected by the addition of the dopant in accordance with the AFM height distribution data in **Figure 5b**.

Figure 6a shows AFM images for the pristine (0 mol%) and n-doped (0.1-2 mol%) NDI3HU-DTYM2 spin-coated layers. The crystalline nature of these layers can be clearly seen in the AFM images, which show a terraced topography. Analysis of the height distribution profiles (**Figure 6b)** of the different layers reveals the presence of several peaks indicated as 1st, 2nd 3rd, etc. Each peak represents a different plateau/terrace. The physical location of some representative terraces are highlighted in the AFM images (**Figure 6a**) with the numbers 1, 2, 3, etc. The larger the terrace/plateau, the larger the corresponding peak in the histogram, whilst the narrower the height distribution the flatter the surface of the terrace is. Evidently, the pristine and 0.1% doped layers NDI3HU-DTYM2 exhibit the most well defined distributions.

A further interesting characteristic of the height histograms is the difference between the peaks, which is in the range 2-3 nm (**Figure 6b**). To gain a better understanding of the layer microstructure we performed XRD measurements on pristine and doped NDI3HU-DTYM2 layers (**Figure 6c**). All measurements show similar diffraction patterns with peaks at 2θ = 4.16°, 8.27° and 12.34°, with corresponding *d*-spacings of 2.13, 1.07 and 0.72 nm, in accordance with the literature.[54] Therefore, inter-plateau height difference of ≈2.1 nm measured by AFM (**Figure 6b**) indicates the presence of large monomolecular terraces in agreement with previous studies.[82] Finally, it can be seen that the addition of DMBI-BDZC at 0.1 mol.% leads to an additional peak at 5.70° (indicated by asterisk in

Figure 6c), with a *d*-spacing of 1.55 nm. The intensity of this peak increases with increasing dopant concentration, suggesting that either the packing motif of NDI3HU-DTYM2 changes or that the dopant segregates. The powder diffraction pattern of the dopant, which was calculated from the single crystal data,[49] is shown in **Figure S6** and does not show any peak at 5.70°. As such we believe that the former explanation is more likely. Further work is required to elucidate the origin of this peak and will be the subject of a future investigation.

3. Conclusions

We demonstrated the effectiveness of DBMI-BDZC as a new, non-volatile molecular n-dopant in two electron transporting organic semiconductors, namely the polymer N2200[82] and the small-molecule NDI3HU-DTYM2.[82] Using DFT calculations, OTFT and EPR measurements, we showed that addition of DBMI-BDZC results in n-doping in both semiconductors, in agreement with the theoretically predicted integer charge transfer process anticipated from the energetics of the dopant and the OSCs. Further evidence comes from temperature dependent electron transport measurements, which reveals that n-type doping reduces the activation energy for electrons whilst results to an overall improvement of transistor's operating characteristics including, increasing of the electron mobility and a systematic reduction in the threshold voltage and contact resistance with increasing DBMI-BDZC concentration. Importantly, admixing of the n-dopant in solution phase, at optimised concentrations, appears not disrupt the crystallinity of the polymer N2200 layers, although there is some minor influence on the packing motif of NDI3HU-DTYM2. Overall, the work demonstrates DMBI-BDZC as a new n-type dopant for polymers and small molecule organic semiconductors.

4. Experimental Section

DFT Calculations: DFT calculations were performed with the code NWChem[83], the B3LYP exchange-correlation functional, [83,84] and the 6-311+G* orbital basis.[85] The relaxation of molecular structures was typically performed with the 6-31G* and 6-311G* bases. Molecular structures and

isosurfaces of HOMOs and LUMOs were rendered with VESTA.[86] The N2200 polymer was modelled using a dimer of the polymer chain.

Materials: The poly{[N,N'-bis(2-octyldodecyl)-naphthalene-1,4,5,8-bis(dicarboximide)-2,6-diyl]-*alt*-5,5'-(2,2'-bithiophene)} P(NDI2OD-T2) (N2200) was synthesized as reported previously[58] with a molecular weight of 100 Kg/mol and a dispersity of 2.6 as measured by gel permeation chromatography (chlorobenzene, 80 °C) against polystyrene standards. (12a,18a)-5,6,12,12a,13,18,18a,19-Octahydro-5,6-dimethyl-13,18[1',2'] benzenobisbenzimidazo[1,2-b:2',1'-d]benzo[i][2.5] benzodiazocine potassium triflate adduct (DMBI-BDZC) was purchased from Strem Chemicals and used as received. NDI3HU- DTYM2 was supplied by Merck KGaA. The materials used for dielectrics, fluoropolymer poly-(perfluorobutenylvinylether) was purchased from Asahi Glass Corp. and the poly(methyl methacrylate) (PMMA) was purchased from Sigma Aldrich (Mw = 120 kD) used without further purification. All materials were stored under nitrogen.

Semiconductor solutions: N2200 was used from a 5mM solution in p-xylene, while the DMBI-BDZC from a 0.2mM in chlorobenzene. NDI3HU- DTYM2 was used from a 9.8mM in mesitylene and the DMBI-BDZC dopant from 1mM in chlorobenzene. For the doped solutions small amounts, calculated by their molar ratio, of the dopant were added into the OSC solutions. For doping of N2200 the molar ratio was calculated versus the mass of the polymer repeat unit. Solutions were heated at 60^{o}C prior to the deposition for 15 minutes.

Transistor Fabrication: Bottom-contact top-gate (BC-TG) transistors were fabricated on glass substrates. 40nm of Au source-drain electrodes were deposited via thermal evaporation in a high vacuum chamber (10^{-6} mbar) through shadow masks, providing transistor devices with channel lengths in the range of 30-100μm and width 1mm. Organic semiconductor solution was then spin coated at 2000 rpm for 30 seconds followed by thermal annealing for 15 minutes at 150^{o}C for the N2200 and 100 ^{o}C for the NDI3HU-DTYM2 devices. For the N2200 and NDI3HU-DTYM2 OTFT devices ~ 500 nm of PMMA and ~ 900 nm of CYTOP were used as dielectric, respectively. Finally,

40 nm of Al was thermally evaporated to form the gate electrode of the transistors. Solution preparation and transistor fabrication were performed in a nitrogen filled glovebox.

Electrical characterization: Transistor characterization was carried out using an Agilent B920A semiconductor parameter analyser in a nitrogen filled glovebox. Low temperature (77 K) transistor measurements were performed using an Agilent B2902A source measure unit where transistor devices were in a cryogenic probe station (Janis Research, ST-500). The linear mobility was calculated using **Eq.2**:

$$\mu_{Lin} = \frac{L}{WC_iV_D}\left(\frac{\partial I_{D,l}}{\partial V_G}\right) \quad (2)$$

where *L* and *W* are the channel length and width of the devices, C_i is the dielectric capacitance and V_D is the drain voltage. The saturation mobility was calculated by using **Eq.3**, where the second derivative of the $I_{D,Sat}$ versus V_G was extracted from the slope of the $I_{D,Sat}^{1/2}$ versus V_G.

$$\mu_{Sat} = \frac{L}{WC_iV_D}\left(\frac{\partial^2 I_{D,S}}{\partial V_G^2}\right) \quad (3)$$

The effective mobility was extracted from the linear regime using **Eq.4**[75]:

$$\mu_{eff} = \frac{L}{WC_iV_D}\left(\frac{I_{D,Lin}}{V_G - V_{ON}}\right) \quad (4)$$

where V_{ON} is the onset voltage which was extracted from the transfer characteristics. In the case of multiple trapping and release model, μ_{eff} provides a physically meaningful V_G dependent value as it represents the average over trapped and free electrons.

Layer surface characterization: Tapping mode was used for the topography AFM images using an Agilent 5500. Image processing and statistical information were extracted using the Gwyddion software.

X-Ray Diffraction: Organic semiconductor solutions were deposited onto silicon substrates. Wide-angle XRD was carried out using a PANalaytical X'Pert Pro MPD with Cu Kα (0.154 nm) emission.

Electron paramagnetic resonance (EPR): Thin films of the pristine and doped organic semiconducting solutions were prepared by drop casting on glass substrates. The EPR spectra were measured using 5 G modulation amplitude, 100 kHz modulation frequency and 25 dB microwave

attenuation. All spectra were measured at low temperatures which were achieved using liquid helium. A Bruker x-band continuous wave EMX PLUS spectrometer was used to record all of the EPR spectra, where the latter was operated at (9.384688) GHz with a standard resonator, CW-EPR, allowing for high sensitivity signal detection.

Acknowledgements

J.P., A.F.P., M.H., and T.D.A acknowledge financial support from the Engineering and Physical Sciences Research Council (EPSRC) (grant EP/L016702/1) and from the European Research Council (ERC) AMPRO project no. 280221. L.T. acknowledges support for the computational time granted from the Greek Research & Technology Network (GRNET) in the National HPC facility – ARIS – under project pr006055-STEM-2. M.H. acknowledges support from the Royal Society. T.D.A acknowledges financial support from the King Abdullah University of Science and Technology (KAUST).

Received: ((will be filled in by the editorial staff))
Revised: ((will be filled in by the editorial staff))
Published online: ((will be filled in by the editorial staff))

References

[1] M. Mizukami, S.-I. Cho, K. Watanabe, M. Abiko, Y. Suzuri, S. Tokito, J. Kido, *IEEE Electron Device Lett.* **2018**, *39*, 39.

[2] W. Zeng, H. Y. Lai, W. K. Lee, M. Jiao, Y. J. Shiu, C. Zhong, S. Gong, T. Zhou, G. Xie, M. Sarma, K. T. Wong, C. C. Wu, C. Yang, *Adv. Mater.* **2018**, *30*, 1704961.

[3] X. Li, J. Zhang, Z. Zhao, L. Wang, H. Yang, Q. Chang, N. Jiang, Z. Liu, Z. Bian, W. Liu, Z. Lu, C. Huang, *Adv. Mater.* **2018**, *30*, 1705005.

[4] J. Hou, O. Inganäs, R. H. Friend, F. Gao, *Nat. Mater.* **2018**, *17*, 119.

[5] J. B. Park, M. Isik, H. J. Park, I. H. Jung, D. Mecerreyes, D. H. Hwang, *ACS Appl. Mater. Interfaces* **2018**, *10*, 4887.

[6] S. D. Ogier, H. Matsui, L. Feng, M. Simms, M. Mashayekhi, J. Carrabina, L. Terés, S. Tokito, *Org. Electron. physics, Mater. Appl.* **2018**, *54*, 40.

[7] Z. Lin, X. Guo, L. Zhou, C. Zhang, J. Chang, J. Wu, J. Zhang, *Org. Electron. physics, Mater. Appl.* **2018**, *54*, 80.

[8] S. Wang, J. Xu, W. Wang, G. J. N. Wang, R. Rastak, F. Molina-Lopez, J. W. Chung, S. Niu, V. R. Feig, J. Lopez, T. Lei, S. K. Kwon, Y. Kim, A. M. Foudeh, A. Ehrlich, A. Gasperini, Y.

Yun, B. Murmann, J. B. H. Tok, Z. Bao, *Nature* **2018**, *555*, 83.

[9] Z. Fei, L. Chen, Y. Han, E. Gann, A. S. R. Chesman, C. R. McNeill, T. D. Anthopoulos, M. Heeney, A. Pietrangelo, *J. Am. Chem. Soc.* **2017**, *139*, 8094.

[10] Y. Xu, H. Sun, A. Liu, H.-H. H. Zhu, W. Li, Y.-F. F. Lin, Y.-Y. Y. Noh, *Adv. Mater.* **2018**, *30*, 1801830.

[11] J. Hu, S. Hu, C. Lu, Y. Huang, K. Xu, X. Wang, *Opt. Mater. (Amst).* **2018**, *75*, 513.

[12] T. Jiang, F. Wang, C. Tang, X. Zhang, X. Cao, Y. Tao, W. Huang, *Dye. Pigment.* **2018**, *150*, 130.

[13] F. Huang, P. I. Shih, C. F. Shu, Y. Chi, A. K. Y. Jen, *Adv. Mater.* **2009**, *21*, 361.

[14] W. S. Jeon, T. J. Park, S. Y. Kim, R. Pode, J. Jang, J. H. Kwon, *Org. Electron.* **2009**, *10*, 240.

[15] F. A. Larrain Benavides, C. Hernandez, W.-F. Chou, V. Rodriguez-Toro, T.-Y. Huang, M. F. Toney, B. Kippelen, *Energy Environ. Sci.* **2018**, *11*, 2216.

[16] N. Wijeyasinghe, F. Eisner, L. Tsetseris, Y. Lin, A. Seitkhan, J. Li, F. Yan, O. Solomeshch, N. Tessler, P. Patsalas, T. D. Anthopoulos, *Adv. Funct. Mater.* **2018**, *28*, 1802055.

[17] M. C. Jung, H. Kojima, I. Matsumura, H. Benten, M. Nakamura, *Org. Electron.* **2018**, *52*, 17.

[18] N. Shintaku, M. Hiramoto, S. Izawa, *J. Phys. Chem. C* **2018**, *122*, 5248.

[19] A. F. Paterson, S. Singh, K. J. Fallon, T. Hodsden, Y. Han, B. C. Schroeder, H. Bronstein, M. Heeney, I. McCulloch, T. D. Anthopoulos, *Adv. Mater.* **2018**, *30*, 1801079.

[20] A. F. Paterson, Y.-H. Lin, A. D. Mottram, Z. Fei, M. R. Niazi, A. R. Kirmani, A. Amassian, O. Solomeshch, N. Tessler, M. Heeney, T. D. Anthopoulos, *Adv. Electron. Mater.* **2018**, *4*, 1700464.

[21] J. T. E Quinn, J. Zhu, X. Li, J. Wang, Y. Li, *J. Mater. Chem. C* **2017**, *5*, 8654.

[22] M. Nikolka, I. Nasrallah, B. Rose, M. K. Ravva, K. Broch, D. Harkin, J. Charmet, M. Hurhangee, A. Brown, S. Illig, P. Too, J. Jongman, I. McCulloch, J.-L. Bredas, H. Sirringhaus, *Nat. Mater.* **2016**, *16*, 356.

[23] D. Kiefer, A. Giovannitti, H. Sun, T. Biskup, A. Hofmann, M. Koopmans, C. Cendra, S. Weber, L. J. Anton Koster, E. Olsson, J. Rivnay, S. Fabiano, I. McCulloch, C. Müller, *ACS Energy Lett.* **2018**, *3*, 278.

[24] S. Yoo, J. Kim, *Macromol. Rapid Commun.* **2015**, *36*, 984.

[25] K. Walzer, B. Maennig, M. Pfeiffer, K. Leo, *Chem. Rev.* **2007**, *107*, 1233.

[26] A. F. Paterson, N. D. Treat, W. Zhang, Z. Fei, G. Wyatt-Moon, H. Faber, G. Vourlias, P. A. Patsalas, O. Solomeshch, N. Tessler, M. Heeney, T. D. Anthopoulos, *Adv. Mater.* **2016**, *28*, 7791.

[27] J. Panidi, A. F. Paterson, D. Khim, Z. Fei, Y. Han, L. Tsetseris, G. Vourlias, P. A. Patsalas, M.

Heeney, T. D. Anthopoulos, *Adv. Sci.* **2018**, *5*, 1700290.

[28] J. L. Hou, D. Kasemann, J. Widmer, A. A. Gunther, B. Lussem, K. Leo, *Appl. Phys. Lett.* **2016**, *108*, 103303.

[29] M. P. Hein, A. A. Zakhidov, B. Lussem, J. Jankowski, M. L. Tietze, M. K. Riede, K. Leo, *Appl. Phys. Lett.* **2014**, *104*, 013507.

[30] E. F. Aziz, A. Vollmer, S. Eisebitt, W. Eberhardt, P. Pingel, D. Neher, N. Koch, *Adv. Mater.* **2007**, *19*, 3257.

[31] B. Nell, K. Ortstein, O. V. Boltalina, K. Vandewal, *J. Phys. Chem. C* **2018**, *122*, 11730.

[32] C. Liu, J. Jang, Y. Xu, H. J. Kim, D. Khim, W. T. Park, Y. Y. Noh, J. J. Kim, *Adv. Funct. Mater.* **2015**, *25*, 758.

[33] R. Wang, Y. Guo, D. Zhang, H. Zhou, D. Zhao, Y. Zhang, *Macromol. Rapid Commun.* **2018**, *39*, 1700726.

[34] Y. Han, Z. Fei, Y. Lin, J. Martin, F. Tuna, T. D. Anthopoulos, *npj Flex. Electron.* **2018**, *2*, 11.

[35] D. H. Lee, M. Kang, D. H. Lim, Y. Kim, J. Lee, D. Y. Kim, K. J. Baeg, *J. Mater. Chem. C* **2018**, *6*, 5497.

[36] I. Salzmann, G. Heimel, M. Oehzelt, S. Winkler, N. Koch, *Acc. Chem. Res.* **2016**, *49*, 370.

[37] S. Braun, W. R. Salaneck, *Chem. Phys. Lett.* **2007**, *438*, 259.

[38] H. Méndez, G. Heimel, S. Winkler, J. Frisch, A. Opitz, K. Sauer, B. Wegner, M. Oehzelt, C. Röthel, S. Duhm, D. Többens, N. Koch, I. Salzmann, *Nat. Commun.* **2015**, *6*, 8560.

[39] H. Sirringhaus, *Adv. Mater.* **2014**, *26*, 1319.

[40] M. L. Tietze, B. D. Rose, M. Schwarze, A. Fischer, S. Runge, J. Blochwitz-Nimoth, B. Lüssem, K. Leo, J. L. Brédas, *Adv. Funct. Mater.* **2016**, *26*, 3730.

[41] T. Menke, D. Ray, J. Meiss, K. Leo, M. Riede, *Appl. Phys. Lett.* **2012**, *100*, 093304.

[42] Z. Bin, Z. Liu, Y. Qiu, L. Duan, *Adv. Opt. Mater.* **2018**, *6*, 1800536.

[43] M. L. Tietze, J. Benduhn, P. Pahner, B. Nell, M. Schwarze, H. Kleemann, M. Krammer, K. Zojer, K. Vandewal, K. Leo, *Nat. Commun.* **2018**, *9*, 1182.

[44] S. P. Schießl, H. Faber, Y. Lin, S. Rossbauer, Q. Wang, K. Zhao, A. Amassian, J. Zaumseil, T. D. Anthopoulos, *Adv. Mater.* **2016**, *28*, 3952.

[45] B. D. Naab, S. Guo, S. Olthof, E. G. B. Evans, P. Wei, G. L. Millhauser, A. Kahn, S. Barlow, S. R. Marder, Z. Bao, *J. Am. Chem. Soc.* **2013**, *135*, 15018.

[46] S. Rossbauer, C. Muller, T. D. Anthopoulos, *Adv. Funct. Mater.* **2014**, *24*, 7116.

[47] P. Wei, J. H. Oh, G. Dong, Z. Bao, *J. Am. Chem. Soc.* **2010**, *132*, 8852.

[48] J. Kim, D. Khim, K. J. Baeg, W. T. Park, S. H. Lee, M. Kang, Y. Y. Noh, D. Y. Kim, *Adv. Funct. Mater.* **2016**, *26*, 7886.

[49] M. S. Jeletic, I. Ghiviriga, K. A. Abboud, A. S. Veige, *Organometallics* **2007**, *26*, 5267.

[50] M. S. Jeletic, R. J. Lowry, J. M. Swails, I. Ghiviriga, A. S. Veige, *J. Organomet. Chem.* **2011**, *696*, 3127.

[51] J. M. Hawkins, A. Meyer, T. A. Lewis, S. Loren, F. J. Hollander, J. M. Hawknis, A. Meyer, T. A. Lewis, S. Loren, F. J. Hollander, *Science (80-.).* **1991**, *253*, 312.

[52] H. E. Winberg, J. R. Downing, D. D. Coffman, *J. Am. Chem. Soc.* **1965**, *87*, 2054.

[53] T. Takenobu, T. Takano, M. Shiraishi, Y. Murakami, M. Ata, H. Kataura, Y. Achiba, Y. Iwasa, *Nat. Mater.* **2003**, *2*, 683.

[54] F. Zhang, Y. Hu, T. Schuettfort, C. Di, X. Gao, C. R. McNeill, L. Thomsen, S. C. B. Mannsfeld, W. Yuan, H. Sirringhaus, D. Zhu, *J. Am. Chem. Soc.* **2013**, *135*, 2338.

[55] K.-J. Baeg, D. Khim, S.-W. Jung, M. Kang, I.-K. You, D.-Y. Kim, A. Facchetti, Y.-Y. Noh, *Adv. Mater.* **2012**, *336*, 327.

[56] S. Gao, Y. Hu, Z. Duan, X. Gao, *Chinese J. Chem.* **2016**, *34*, 689.

[57] J. R. Zbieg, E. Yamaguchi, E. L. McInturff, M. J. Krische, *Science (80-.).* **2012**, *336*, 327.

[58] H. Yan, Z. Chen, Y. Zheng, C. Newman, J. R. Quinn, F. Dötz, M. Kastler, A. Facchetti, *Nature* **2009**, *457*, 679.

[59] G. J. A. H. Wetzelaer, M. Kuik, Y. Olivier, V. Lemaur, J. Cornil, S. Fabiano, M. A. Loi, P. W. M. Blom, *Phys. Rev. B* **2012**, *86*, 165203.

[60] J. Sun, J. Gu, J. Yuan, Z. Cui, K. Lu, S. Shi, G. Ding, W. Ma, *Org. Electron.* **2016**, *33*, 227.

[61] C. Mu, P. Liu, W. Ma, K. Jiang, J. Zhao, K. Zhang, Z. Chen, Z. Wei, Y. Yi, J. Wang, S. Yang, F. Huang, A. Facchetti, H. Ade, H. Yan, *Adv. Mater.* **2014**, *26*, 7224.

[62] L. Gao, Z. G. Zhang, L. Xue, J. Min, J. Zhang, Z. Wei, Y. Li, *Adv. Mater.* **2016**, *28*, 1884.

[63] Z. Ding, X. Long, C. Dou, J. Liu, L. Wang, *Chem. Sci.* **2016**, *7*, 6197.

[64] J. C. Blakesley, M. Schubert, R. Steyrleuthner, Z. Chen, A. Facchetti, D. Neher, *Appl. Phys. Lett.* **2011**, *99*, 183310.

[65] C. W. Koh, J. H. Heo, M. A. Uddin, Y. W. Kwon, D. H. Choi, S. H. Im, H. Y. Woo, *ACS Appl. Mater. Interfaces* **2017**, *9*, 43846.

[66] T. Ye, J. Wang, W. Chen, Y. Yang, D. He, *ACS Appl. Mater. Interfaces* **2017**, *9*, 17923.

[67] P. Pingel, M. Arvind, L. Kölln, R. Steyrleuthner, F. Kraffert, J. Behrends, S. Janietz, D. Neher, *Adv. Electron. Mater.* **2016**, *2*, 1600204.

[68] A. Salleo, *Mater. Today* **2007**, *10*, 38.

[69] B. Lüssem, C. M. Keum, D. Kasemann, B. Naab, Z. Bao, K. Leo, *Chem. Rev.* **2016**, *116*, 13714.

[70] A. F. Paterson, S. Singh, K. J. Fallon, T. Hodsden, Y. Han, B. C. Schroeder, H. Bronstein, M.

Heeney, I. McCulloch, T. D. Anthopoulos, *Adv. Mater.* **2018**, *30*, 1801079.

[71] S. K. Possanner, K. Zojer, P. Pacher, E. Zojer, F. Schürrer, *Adv. Funct. Mater.* **2009**, *19*, 958.

[72] Z. A. Lamport, K. J. Barth, H. Lee, E. Gann, S. Engmann, H. Chen, M. Guthold, I. McCulloch, J. E. Anthony, L. J. Richter, D. M. DeLongchamp, O. D. Jurchescu, *Nat. Commun.* **2018**, *9*, 5130.

[73] D. Braga, M. Ha, W. Xie, C. D. Frisbie, *Appl. Phys. Lett.* **2010**, *97*, 193311.

[74] Dieter K. Schroder, *Semiconductor Material and Device Characterization, 3rd Edition*; Third Edit.; Wiley-IEEE Press, 2015.

[75] S. Hunter, J. Chen, T. D. Anthopoulos, *Adv. Funct. Mater.* **2014**, *24*, 5969.

[76] M. Gruber, S. H. Jung, S. Schott, D. Venkateshvaran, A. J. Kronemeijer, J. W. Andreasen, C. R. McNeill, W. W. H. Wong, M. Shahid, M. Heeney, J. K. Lee, H. Sirringhaus, *Chem. Sci.* **2015**, *6*, 6949.

[77] R. A. Street, J. E. Northrup, A. Salleo, *Phys. Rev. B* **2005**, *71*, 165202.

[78] R. Noriega, J. Rivnay, K. Vandewal, F. P. V Koch, N. Stingelin, P. Smith, M. F. Toney, A. Salleo, *Nat. Mater.* **2013**, *12*, 1038.

[79] S. Olthof, S. Mehraeen, S. K. Mohapatra, S. Barlow, V. Coropceanu, J.-L. Brédas, S. R. Marder, A. Kahn, *Phys. Rev. Lett.* **2012**, *109*, 176601.

[80] G. Horowitz, P. Delannoy, *J. Appl. Phys.* **1991**, *70*, 469.

[81] Y.-H. Lin, H. Faber, S. Rossbauer, T. D. Anthopoulos, *Appl. Phys. Lett.* **2013**, *102*, 193516.

[82] F. Zhang, C. Di, N. Berdunov, Y. Hu, Y. Hu, X. Gao, Q. Meng, H. Sirringhaus, D. Zhu, *Adv. Mater.* **2013**, *25*, 1401.

[83] M. Valiev, E. J. Bylaska, N. Govind, K. Kowalski, T. P. Straatsma, H. J. J. Van Dam, D. Wang, J. Nieplocha, E. Apra, T. L. Windus, W. A. de Jong, *Comput. Phys. Commun.* **2010**, *181*, 1477.

[84] P. J. Stephens, F. J. Devlin, C. F. Chabalowski, M. J. Frisch, *J. Phys. Chem.* **1994**, *98*, 11624.

[85] R. Krishnan, J. S. Binkley, R. Seeger, J. A. Pople, *J. Chem. Phys.* **1980**, *72*, 650.

[86] K. Momma, F. Izumi, *J. Appl. Crystallogr.* **2011**, *44*, 1272.

https://doi.org/10.1002/adfm.201902784

Figures

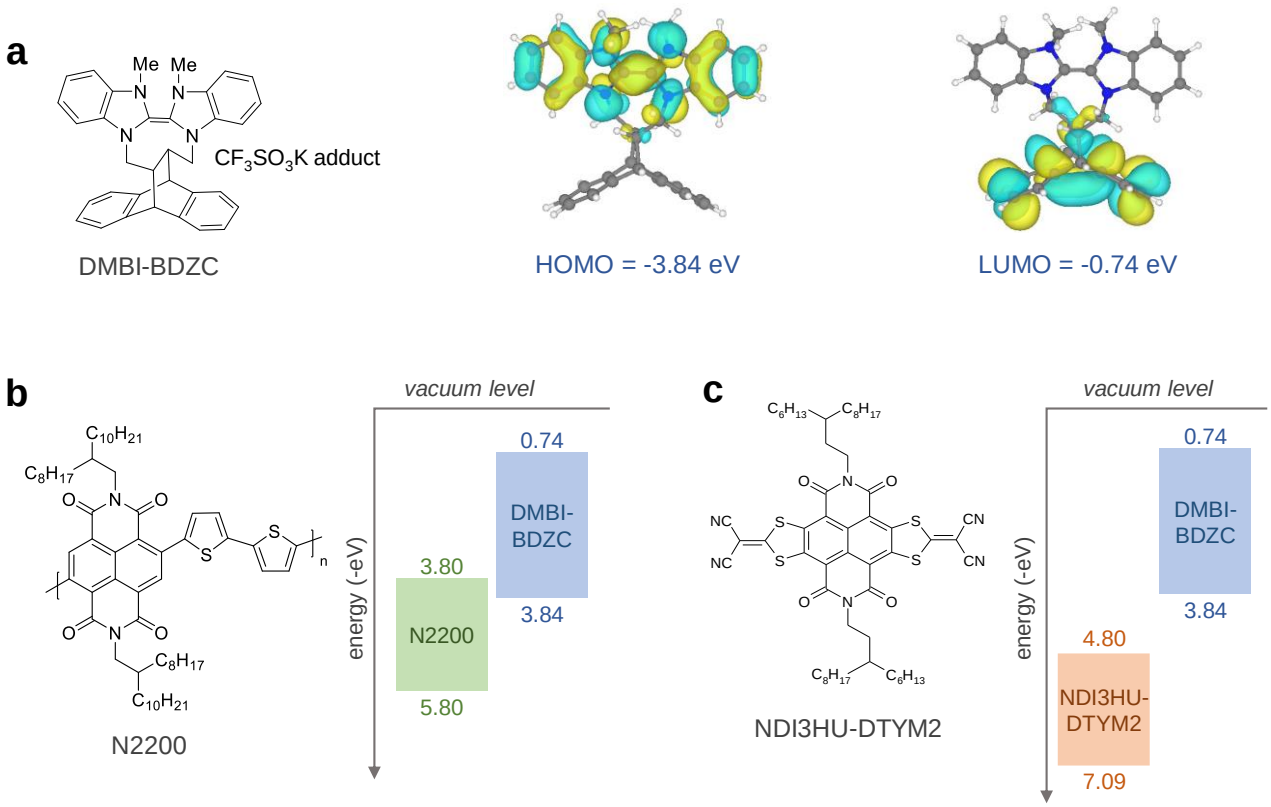

Figure 1. (a) Chemical structures of DMBI-BDZC along with the HOMO and LUMO energy levels as calculated via DFT. Molecular structures of the polymer N2200 (b) and the small molecule NDI3HU-DTYM2 (c), together with their energy levels plotted along those of DMBI-BDZC.

https://doi.org/10.1002/adfm.201902784

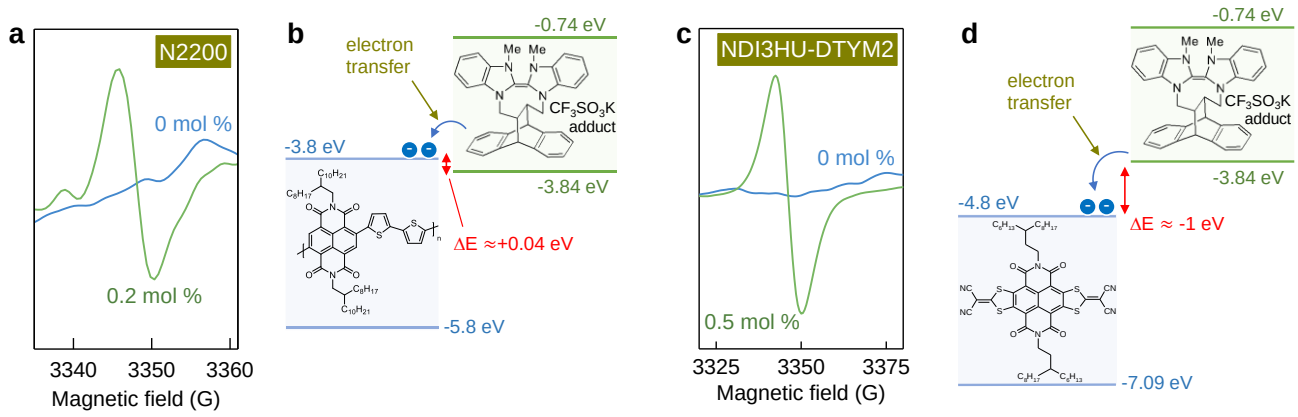

Figure 2. Electron paramagnetic resonance measurements for the (a) N2200:DMBI-BDZC pristine (0 mol%) & doped (0.2 mol%) and (c) NDI3HU-DTYM2:DMBI-BDZC pristine (0 mol%) & doped (0.5 mol%). Electron transfer mechanism for the (b) N2200:DMBI-BDZC and (d) NDI3HU-DTYM2:DMBI-BDZC systems.

https://doi.org/10.1002/adfm.201902784

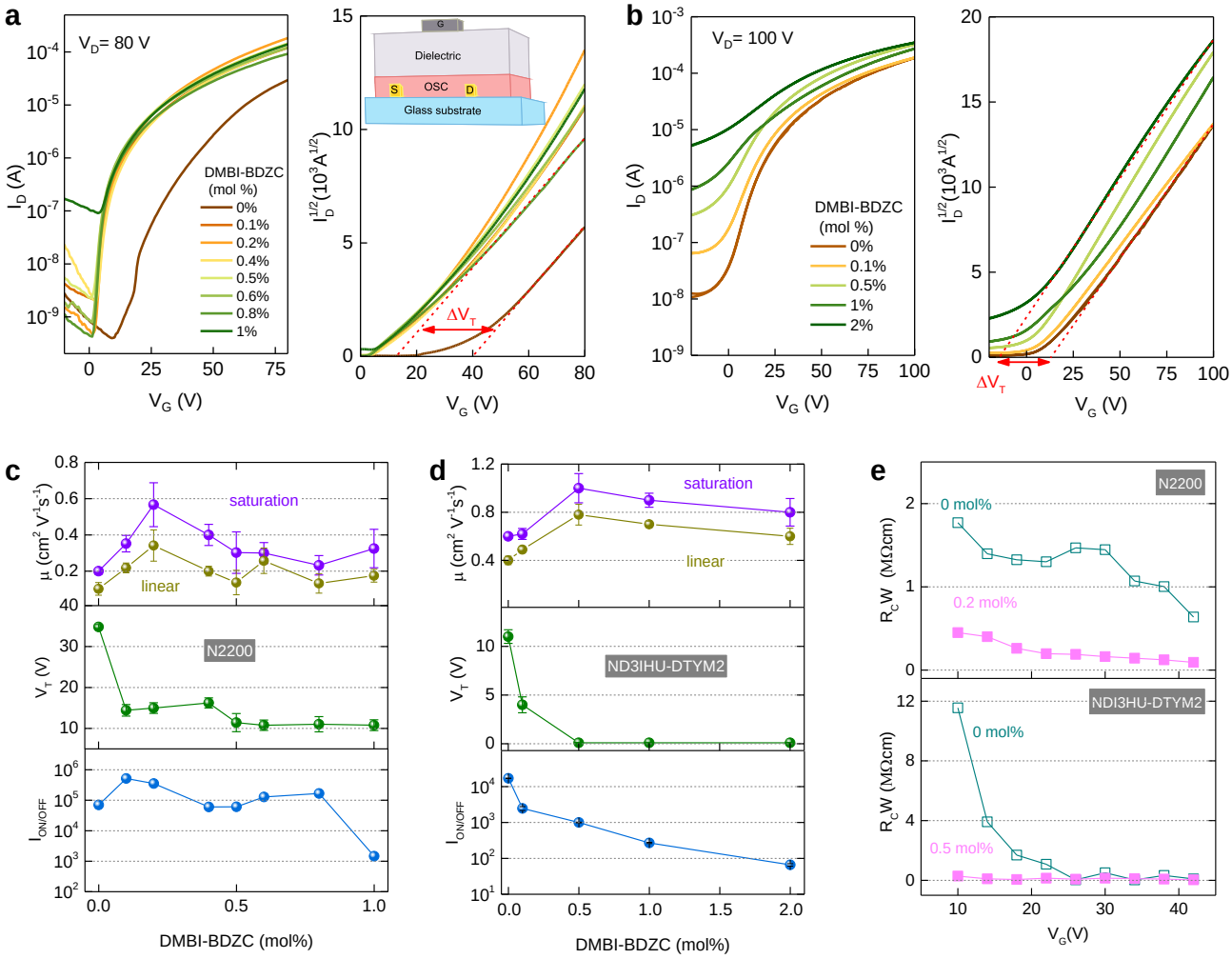

Figure 3. Transfer characteristics of BC-TG (a) N2200:DMBI-BDZC and (b) NDI3HU-DTYM2:DMBI-BDZC OTFTs on increasing dopant concentration (mol%) with their corresponding square root I_D vs V_G plots. Electron mobility (μ) in linear and saturation regime and threshold voltage (V_T) variation as a function of the DMBI-BDZC mol% and $I_{ON/OFF}$ ratio for (c) N2200:DMBI-BDZC and (d) NDI3HU-DTYM2:DMBI-BDZC. (e) Contact resistance (R_C) as extracted from the TLM method for the N2200:DMBI-BDZC and NDI3HU-DTYM2:DMBI-BDZC OTFTs. (OTFTs with channel width 1000 and length 40 μm).

https://doi.org/10.1002/adfm.201902784

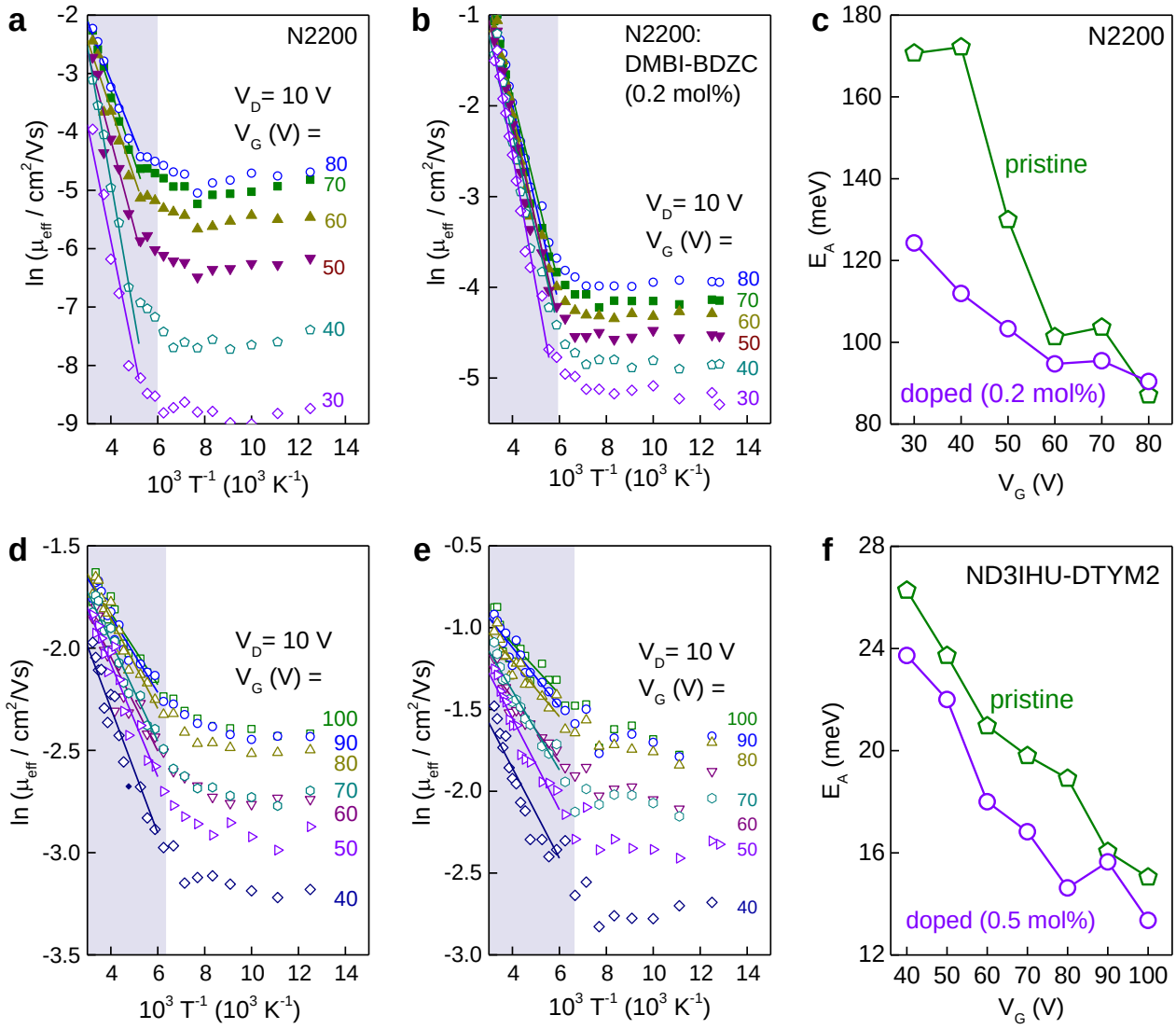

Figure 4. Arrhenius plots of N2200:DMBI-BDZC OTFTs with channel width 1000 and length 40 μm for (a) 0 mol% & (b) 0.2 mol% and NDI3HU-DTYM2:DMBI-BDZC with channel width 1000 and length 30 μm for (c) 0 mol% and (d) 0.5 mol%, as extracted from OTFTs when measured by applying V_D= 10 V. Activation energy E_A as function of V_G, as extracted from (a-d) for (e) N2200:DMBI-BDZC and (f) NDI3HU-DTYM2:DMBI-BDZC OTFTs.

https://doi.org/10.1002/adfm.201902784

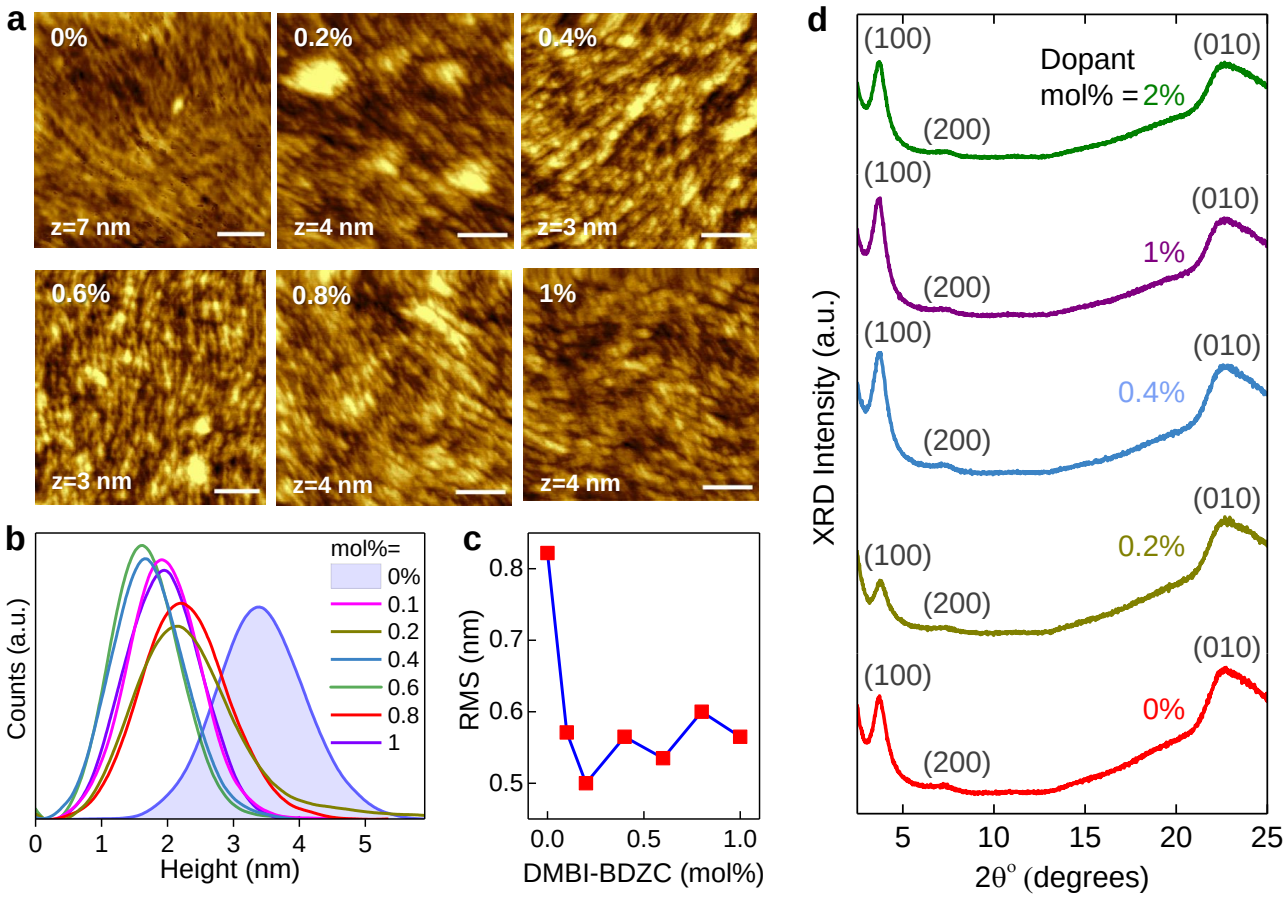

Figure 5. Thin film morphological analysis for N2200:DMBI-BDZC (0-1 mol%) (a) Topography AFM images of thin films, (b) their corresponding height histogram and (c) the surface roughness (RMS) as a function of DMBI-BDZC mol%, as extracted from the topography scans. (d) XRD patterns for the 0-2 mol% N2200:DMBI-BDZC thin films.

https://doi.org/10.1002/adfm.201902784

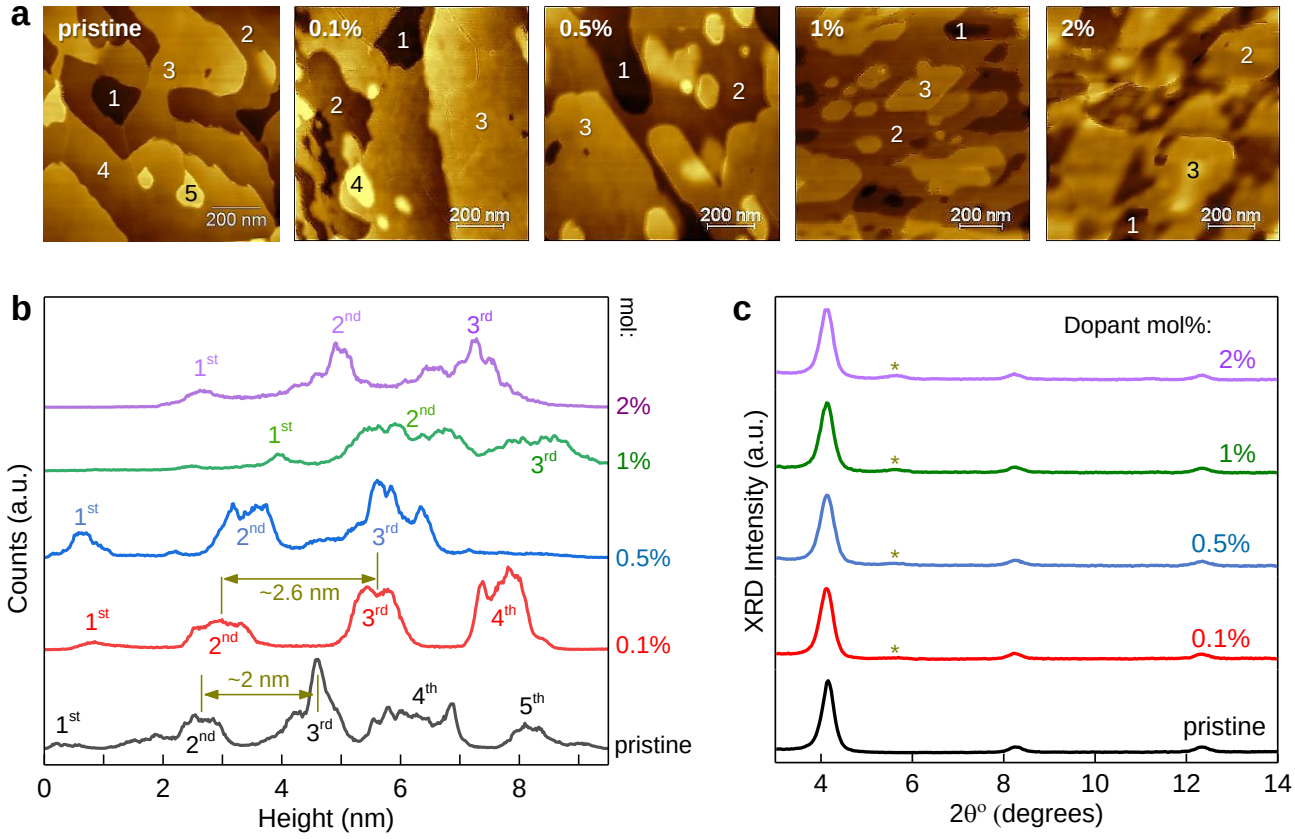

Figure 6. Thin film morphological analysis for NDI3HU-DTYM2:DMBI-BDZC (0-2 mol%) (a) Topography AFM images of thin films, and (b) their corresponding height histogram. (c) XRD patterns for the 0-2 mol% NDI3HU-DTYM2:DMBI-BDZC thin films.

https://doi.org/10.1002/adfm.201902784

ToC Text

We introduce the new non-volatile n-type molecular dopant DMBI-BDZC and demonstrate its ability to improve the operating characteristics of high mobility n-channel organic transistors based on the polymer N2200 and the small-molecule NDI3HU-DTYM2. Doping via the ground-state electron transfer process reduces the activation energy for electron transport, increases the electron mobility and reduces the contact resistance in both transistors.

Keywords: organic semiconductors; organic transistor; electron transport; molecular doping; n-type dopant

Julianna Panidi, Jaspreet Kainth, Alexandra F. Paterson, Simeng Wang, Leonidas Tsetseris, Abdul-Hamid Emwas, Martyn A. McLachlan, Martin Heeney, Thomas D. Anthopoulos**

Introducing a Non-Volatile N-Type Dopant Drastically Improves Electron Transport in Polymer and Small-Molecule Organic Transistors

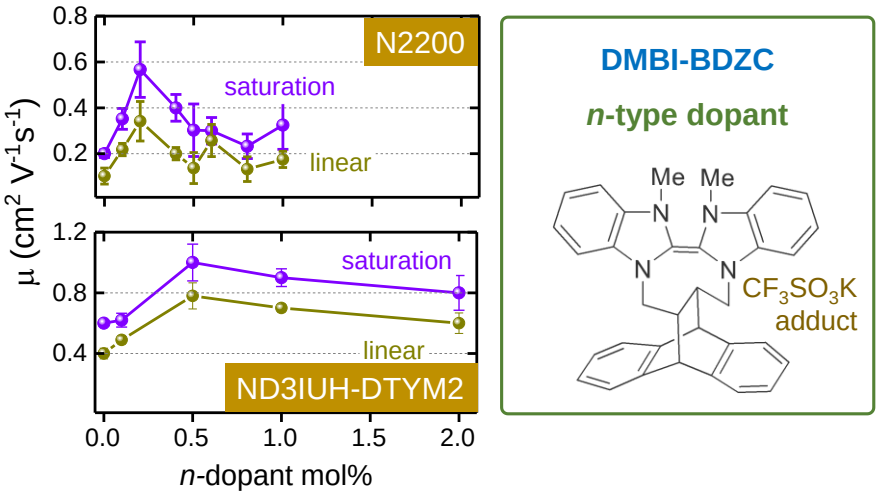

https://doi.org/10.1002/adfm.201902784

Supporting Information

Introducing a Non-Volatile N-Type Dopant Drastically Improves Electron Transport in Polymer and Small-Molecule Organic Transistors

Julianna Panidi, Jaspreet Kainth, Alexandra F. Paterson, Simeng Wang, Leonidas Tsetseris, Abdul-Hamid Emwas, Martyn A. McLachlan, Martin Heeney, Thomas D. Anthopoulos**

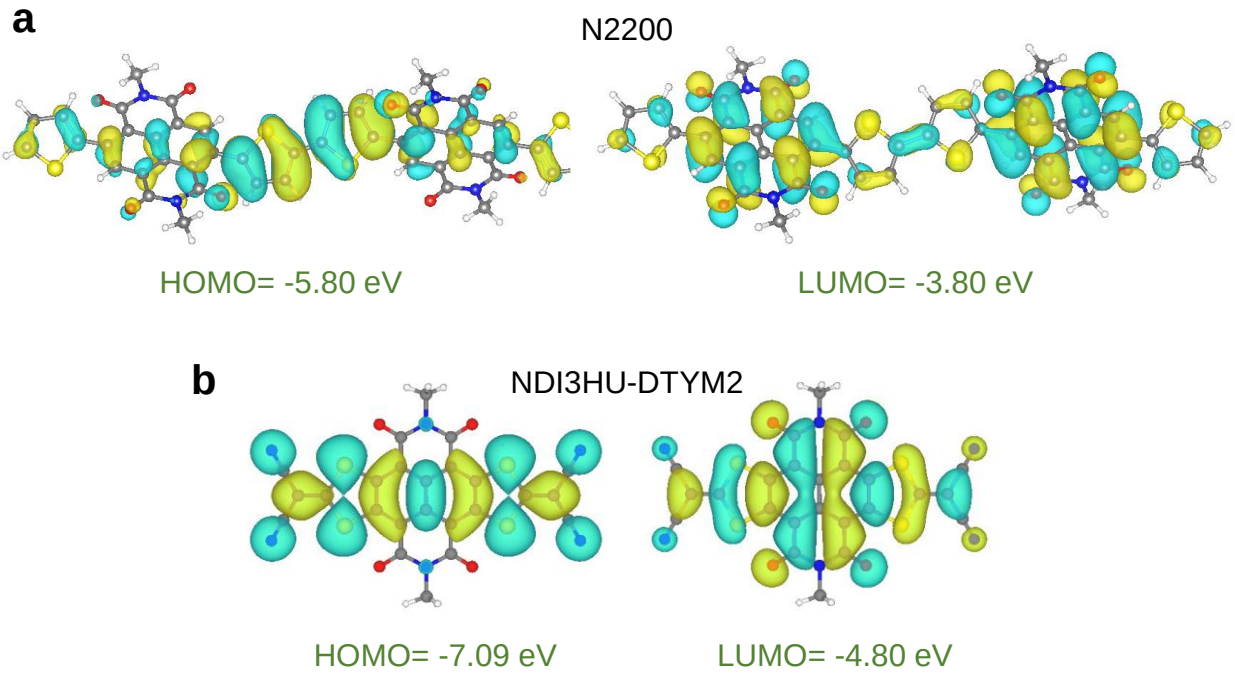

Figure S1. Lowest unoccupied molecular orbital (LUMO) and highest occupied molecular orbital (HOMO) energies for (a) N2200 and (b) NDI3HU-DTYM2 as calculated via the DFT method.

https://doi.org/10.1002/adfm.201902784

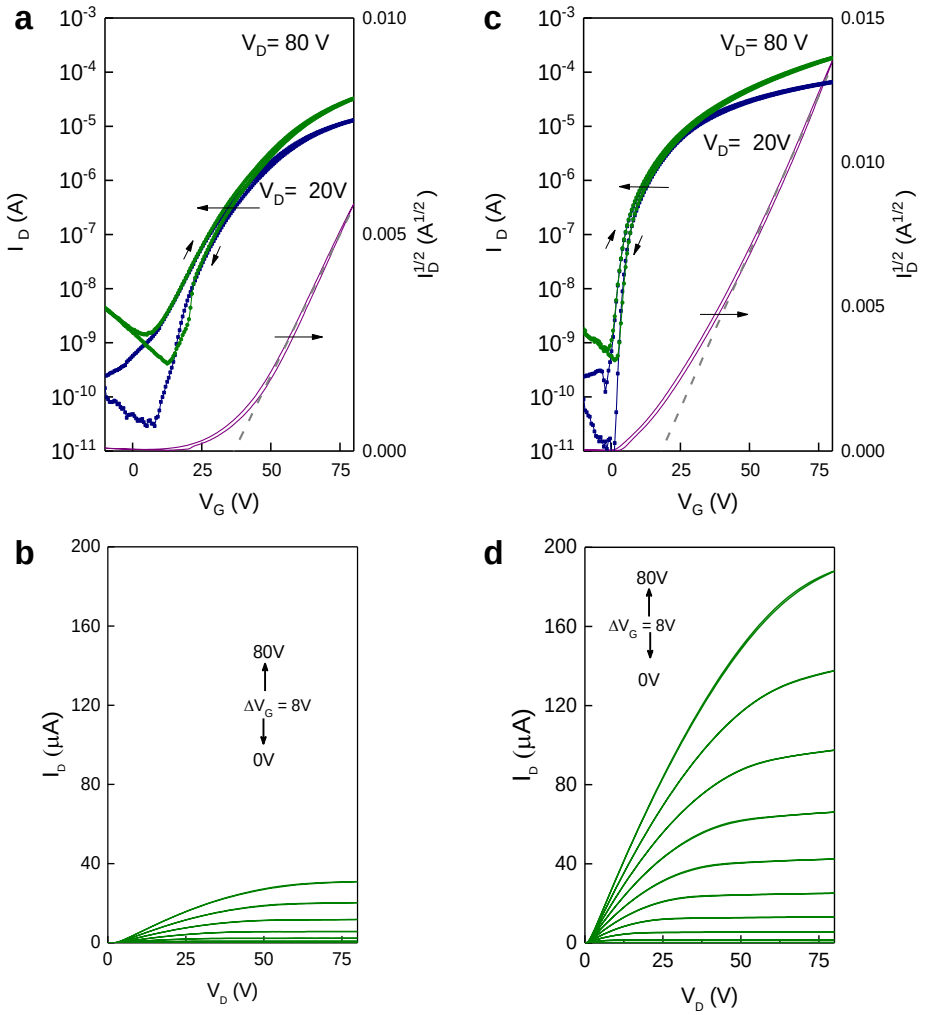

Figure S2. Representative transfer (top) and output (bottom) characteristics of N2200:DMBI-BDZC (a-b) pristine (0 mol%) and (c-d) 0.2 mol% doped N2200 transistors, with channel length of 40 and width of 1000 μm.

https://doi.org/10.1002/adfm.201902784

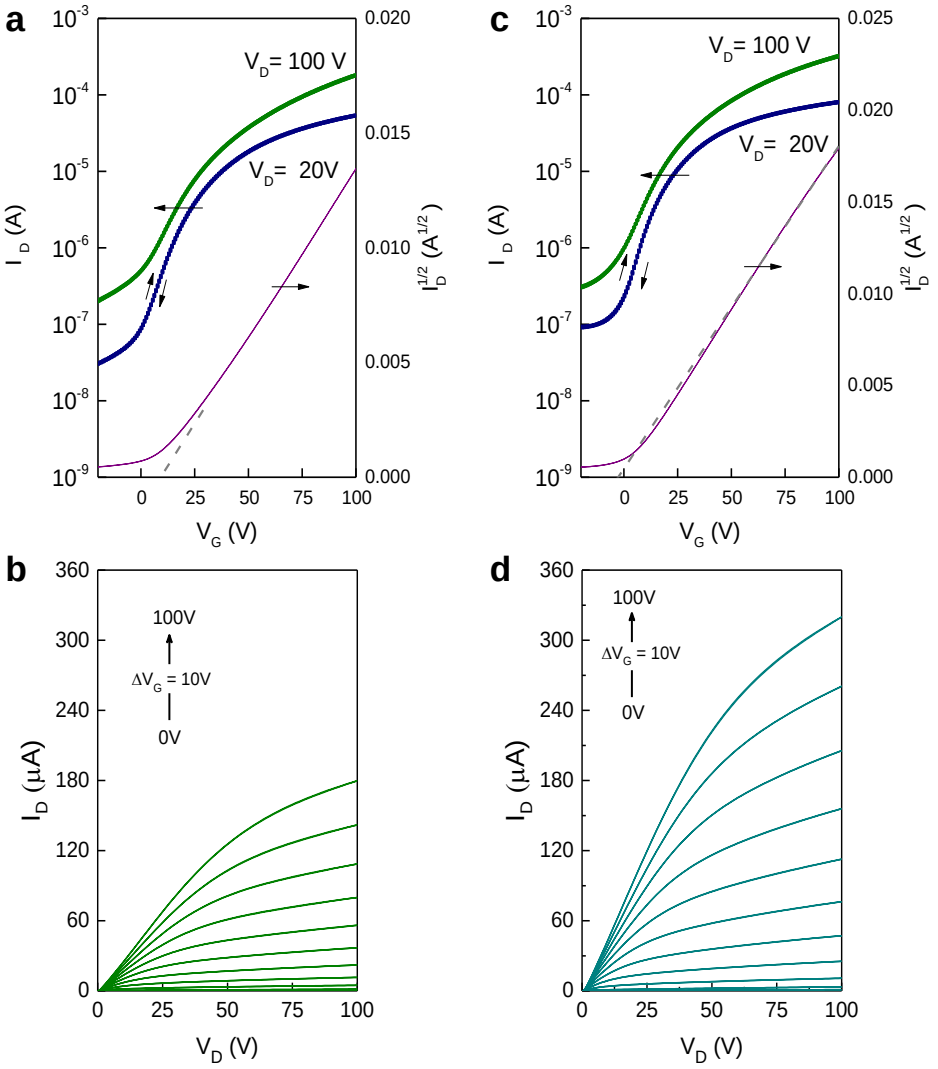

Figure S3. Representative transfer (top) and output (bottom) characteristics of pristine and DMBI-BDZC-doped NDI3HU-DTYM2 OTFTs. (a-b) pristine (0 mol%) and (c-d) 0.5 mol% DMBI-BDZC-doped NDI3HU-DTYM2 transistors, with channel length of 40 and width of 1000 μm.

https://doi.org/10.1002/adfm.201902784

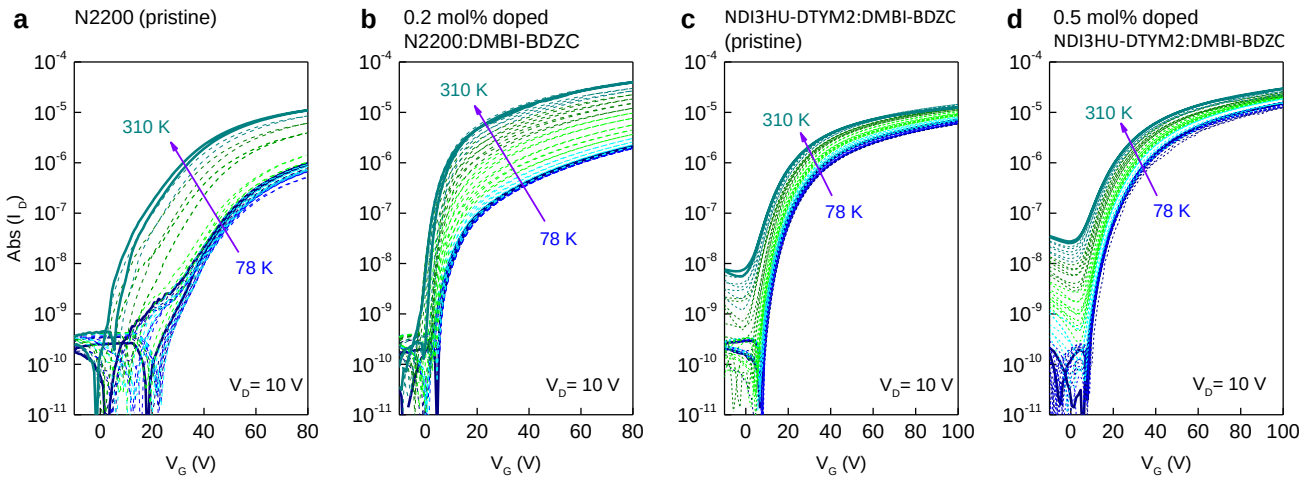

Figure S4. Temperature dependent charge transport measurements performed in the range 78-310 K. Transfer characteristics of (a) pristine and (b) 0.2 mol% DMBI-BDZC-doped N2200 OTFTs, with channel width 1000 µm and length 40 µm. Transfer characteristics of (c) pristine and (d) 0.5 mol% DMBI-BDZC-doped NDI3HU-DTYM2 OTFTs, with channel width and length of 1000 and 30 µm, respectively.

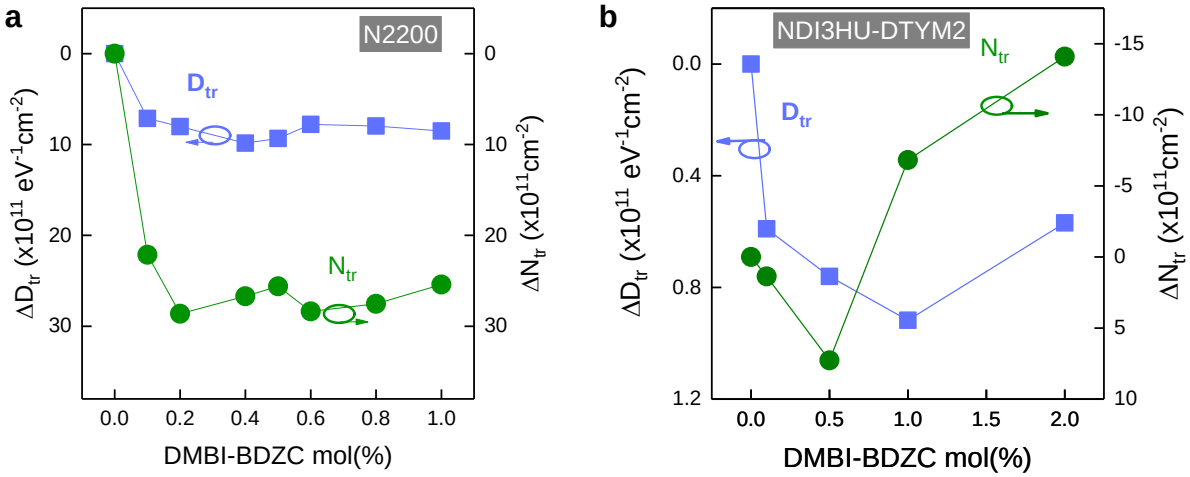

Figure S5: Relative trap density (ΔN_{tr}) and trap concentration (ΔD_{tr}) for the (a) N200:DMBI-BDZC and (b) NDI3HU-DTYM2:DMBI-BDZC devices as calculated from the transfer curves. The equations for these calculations were adapted from the literature.[81]

https://doi.org/10.1002/adfm.201902784

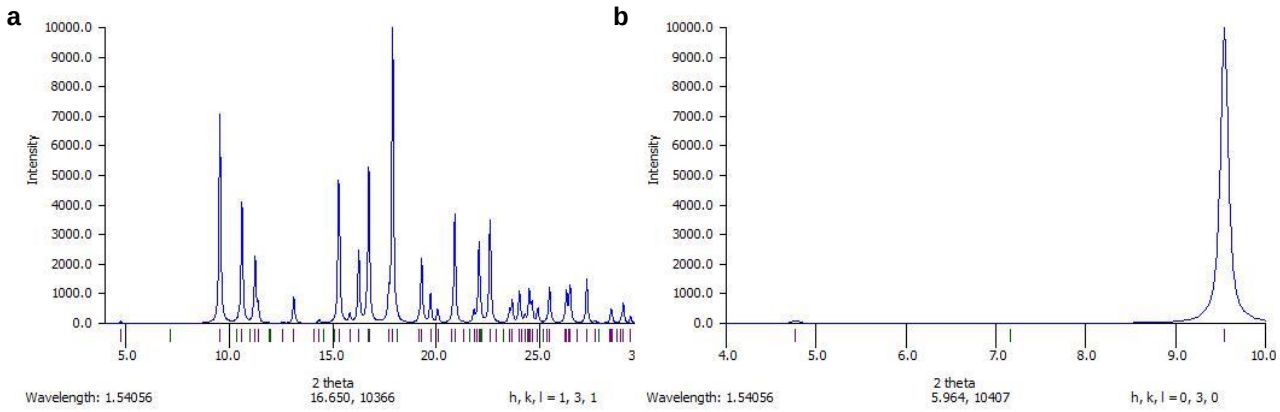

Figure S6: Calculated XRD pattern of the dopant DMBI-BDZC (a) from 4º to 30 º and (b) from 4º to 10 º in 2θ.